

Water Resources Research®



RESEARCH ARTICLE

10.1029/2023WR035990

Key Points:

- Persistent cohomology can be used to summarize topographic information
- A persistence threshold is adequate to identify berms and stock ponds from focused regions
- A set of criteria calculated from persistence can detect 64% of observed berms

Supporting Information:

Supporting Information may be found in the online version of this article.

Correspondence to:

D. A. Lapides,
danalapides@gmail.com

Citation:

Lapides, D. A., Grindstaff, G., & Nichols, M. H. (2024). Automated earthwork detection using topological persistence. *Water Resources Research*, 60, e2023WR035990. <https://doi.org/10.1029/2023WR035990>

Received 16 AUG 2023

Accepted 20 DEC 2023

Automated Earthwork Detection Using Topological Persistence

Dana A. Lapides¹ , Gillian Grindstaff^{2,3} , and Mary H. Nichols¹

¹Southwest Watershed Research Center, USDA-ARS, Tucson, AZ, USA, ²Department of Mathematics, University of Oxford, Oxford, UK, ³Department of Mathematics, University of California, Los Angeles, CA, USA

Abstract For thousands of years, humans have altered the movement of water through construction of earthworks. These earthworks remain in landscapes, where they continue to alter hydrology, even where structures have long since been abandoned. Management of lands containing earthworks requires an understanding of how the earthworks impact hydrology and knowledge of where the structures are located in the landscape. Various methods for detecting topographic features exist in the literature, including a set of rule and threshold-based techniques and machine learning methods. These tools are either labor-intensive or require special pre-processing or a priori assumptions about structures that limit generalizability. Here, we test a topological analysis tool called “persistence” to determine if it is useful for earthwork detection in rangelands. We found that persistence can be used to detect earthworks with 83% precision and 64% accuracy. Breached berms and berms with significant upslope sedimentation are most likely not to be detected using persistence. These results indicate that persistence can be useful for terrain analysis, and it has the potential to substantially reduce manual effort in feature detection by identifying regions where berms may be found.

Plain Language Summary The shape of landscapes controls how water moves over the surface. Humans have modified landscapes by building earthen structures to direct water for thousands of years. The legacy of human water management systems remains in many places around the world, and land managers need to understand how these structures impact hydrology and where they are in order to support management decisions. Earthen dams, berms, and stock ponds dot the southwestern United States. High-resolution elevation maps and imagery are increasingly available, and although man-made structures are readily visible to the eye, automatic detection remains a challenge. In this study, a method from the mathematical field of topology called “persistence” was applied to automatically detect berms and stock ponds from elevation arrays. This method identifies features from a series of binary images generated from the same elevation map at consecutive threshold values. Results demonstrate that persistence is able to detect well-defined berms. While not all berms are detected, these results are still promising since berms are generally found in groups. Thus, detection of even two thirds of the berms substantially narrows down regions for manual inspection.

1. Introduction

Surface hydrology is a direct reflection of topography, which drives how flows accumulate or spread as water moves downslope. Thus, hydrological processes are impacted by changes in the topographic structure of the landscape. Humans have taken advantage of this for thousands of years (Myers, 1975) to divert natural flows into water storage for farming (e.g., Boers & Ben-Asher, 1982; Bryan, 1929; Campisano et al., 2017; Pandey et al., 2003; Tadmor et al., 1971) or divert floods away from homes or other infrastructure (e.g., Cheng & Chau, 2004; Sills et al., 2008). Such man-made systems have been shown to impact hydrology and ecology of landscapes (Steinfeld & Kingsford, 2013). Thus, as practitioners seek to manage human-impacted landscapes, it is important to characterize the impacts of man-made structures on flows. An important prerequisite to this problem is identifying where existing man-made structures are located in the landscape. This is particularly an issue for earthworks that are constructed from the same material as the surrounding landscape.

While many structures are readily visible from high-resolution imagery or digital terrain models (DTMs) (Tarolli, 2014; Tarolli et al., 2015), the number or size of structures can make manual cataloging by visual inspection of imagery or elevation data a laborious and time-consuming task. Methods for detecting earthworks in agricultural lands (Tarolli et al., 2015) and on floodplains (Steinfeld et al., 2013) are the subject of ongoing research, but less attention has been given to feature identification in rangelands (Nichols et al., 2018). In part, this is because high-resolution data may be less available, but several other challenges make identifying runoff and erosion control structures in rangelands difficult. Many earthworks are small in

comparison with natural landscape features such as mountains and hills, and structures in low relief settings such as floodplains are difficult to distinguish from natural topographic variations. Thus, while earthworks may be obvious to the human eye, finding an automated way to reveal earthworks from imagery or DTMs is challenging.

Terrain analysis algorithms generally rely on DTMs (Wilson et al., 2000) and/or satellite imagery (Xiong et al., 2021) for analysis. Zhou et al. (2019) provides a detailed review of feature identification techniques, in which they classify into a few main types: thresholding, stream/drainage network analysis, visual descriptor detection, and object-based image analysis. Thresholding involves assigning a binary threshold for detection based on a data value at each pixel (e.g., Goldgof et al., 1989, 1990; Molloy & Stepinski, 2007; Naik & Murthy, 2006; Passalacqua et al., 2010). Stream/drainage network analysis uses calculations of flow lines across the landscape to identify flow pathways and ridgelines (e.g., Lindsay & Dhun, 2015; Liu & Zhang, 2011; Saraf et al., 2004; Tarolli et al., 2012; Zhang et al., 2014). These first two methods are the simplest feature detection strategies and generally do not result in satisfactory results for most feature detection tasks, leading to the development of more complex methods (Zhou et al., 2019). Visual descriptors are used to extract interesting points using a variety of different methods to distinguish points from their neighbors or within a pattern (e.g., geomorphons; Jasiewicz & Stepinski, 2013). OBIA takes advantage of segmentation (Arundel, 2016; Drăguț & Eisank, 2012), morphology (Soille & Pesaresi, 2002), and object-based segmentation (Khan & Shah, 2001) methods to cluster pixel data into regions with similar characteristics. Beyond the strategies summarized in Zhou et al. (2019), image processing and pattern techniques have also been applied for terrain analysis, but these algorithms tend to be poorly suited to terrain data, since they are generally not smoothly-varying (Wang & Li, 2021). Machine learning has been recently introduced for feature detection with great success (e.g., Hsu et al., 2021; Steinfeld et al., 2013; Torres et al., 2020; Wang & Li, 2021; with true positive detection rates of about 60%–98%); data preparation for model training, though, can be time-consuming and labor-intensive since training data requires pre-existing data sets that are generally developed using semi-automated or fully manual methods.

Persistent (co)homology (hereafter referred to as “persistence”) is a computational method that allows for topological characterization of complex data at various spatial resolutions without the need for any additional pre-processing or training data preparation. Persistence-based topographical analysis is a natural and powerful tool for overall landscape summary; it simultaneously detects all critical points on the landscape, including depressions, bumps, saddle features, and holes, and expresses this information as a quantifiable object suitable for statistical analysis. As such, persistence has great potential to be used for automated detection of topographic features that impact surface runoff patterns across scales. Of the existing methods for feature detection common in the literature, persistence functions most similarly to visual descriptor techniques, in that it is an algorithm to identify features that stand out from their surroundings. Given that visual descriptor techniques have been shown to be effective, persistence could prove to be a useful tool for feature detection.

Persistence has become an increasingly popular tool for spatial analysis applications (Corcoran & Jones, 2023). In hydrology, persistence has been used to analyze fracture networks (Suzuki et al., 2021), subsurface pore structure (e.g., Herring et al., 2019; Moon et al., 2019), Kolmogorov flow (Kramar et al., 2016), hurricane patterns (Tymochko et al., 2020), cloud development in radar maps (Corcoran, 2019b; Corcoran & Jones, 2018), and to detect critical points in flood early warning systems (Syed Musa et al., 2021). Persistence has also been developed to quantify morphology of 2d and 3d shapes (Chung et al., 2022), for example, to estimate the structural integrity of tunnels (Zhang et al., 2020) and identify morphological differences between leaves of different plant species (Li et al., 2018). In landscape analysis, persistence has been proposed as a method to reduce noise in rasters (Corcoran, 2019a) and to identify landslides (Syzydkbayev et al., 2020b). For more examples of the usage of topological data analysis (TDA) in geospatial contexts, see Corcoran and Jones (2023).

To date, applications of persistence in hydrology have been promising, but persistence remains an under-explored tool for feature detection. In this work, we apply (0-dimensional) persistence to high-resolution gridded elevation data to detect sub-hillslope scale topographic features relevant to surface-water hydrology. We assess whether persistence can be used to detect earthen berms in rangelands in Arizona, USA in (a) a series of proof-of-concept tests with synthetically added berms and (b) four real sites containing a total of 103 manually identified berms.

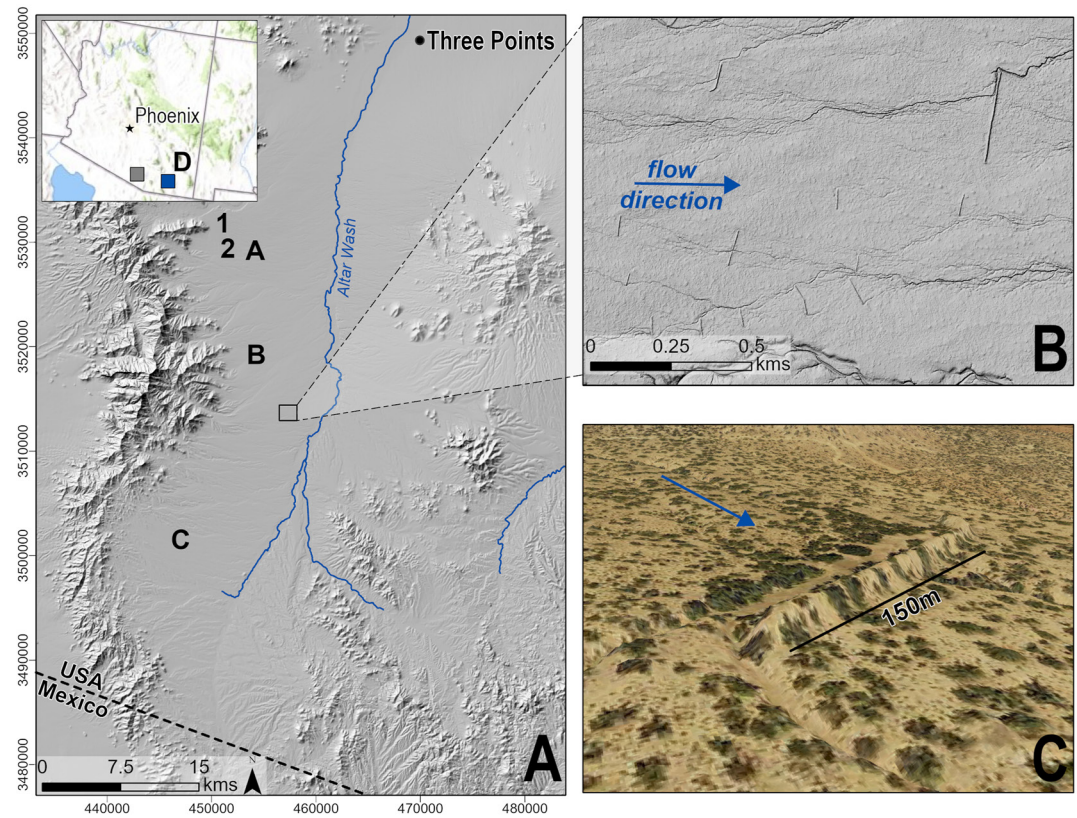


Figure 1. (a) Map showing the locations of the study sites in Arizona, USA. Numbers 1 and 2 are locations of unaltered landscapes. Locations A–D show the locations of the four study sites. Site D is marked with a blue box in the inset. The gray box in the inset marks the location of the hillshade shown in panel (a). (b) Zoomed-in hillshade showing an example of berms on the landscape. (c) Exaggerated height image showing an example berm with the direction of flow indicated with a blue arrow. Hillshades in all panels are based on lidar data from Pima County Flood Control District, and imagery in panel (c) is from Google Earth.

2. Methods

2.1. Study Site

The study site is located in the Altar Valley in southern Arizona, USA (Figure 1). Precipitation in the valley is sparse, and persistent surface water is lacking. More than half of the 415 mm (16.3 in) of mean annual precipitation occurs from July–September during the North American Monsoon (Adams & Comrie, 1997). Runoff generated during monsoon season convective storms provides water that supports livestock production throughout the year. Thus, control over water supplies and distribution is critical for agriculture in the valley. Throughout the valley, surface runoff generated by storms is captured in stock ponds or diverted using earthen berms. Stock ponds typically consist of an excavated basin and an earthen dam to capture water in the basin, while earthen berms were constructed to intercept and reduce the velocity of sheet flow to increase soil moisture and enhance vegetation establishment and growth. Slowing surface runoff has the added advantage of reducing soil erosion, retaining the soils necessary to store moisture and support vegetation.

Earthworks (stock ponds and berms) to manipulate runoff were constructed through time in the valley by multiple land owners and managers and remain on the landscape in varying condition. In some cases, unmaintained structures have deteriorated to the extent that they have caused gulying and increased erosion (Nichols et al., 2018). Currently, the Altar Valley Conservation Alliance is leading an effort to develop large scale collaborative conservation plans to improve watershed function and restore degraded land. Critical to this effort is knowledge of prior landscape and runoff alteration, as well as information on the condition of man-made structures. Thus, tools are needed for identifying and mapping geomorphic structures such as stock ponds and earthen berms. In this study, we focus on identifying berms because there are more berms than stock ponds on the landscape, and stock ponds are generally built with berms to retain water. Thus, identifying berms could allow for stock pond identification.

2.2. Threshold Persistence

Topographic feature detection is a common application in hydrology (e.g., Atkinson et al., 2020; Bonetto et al., 2015; Höfle et al., 2013; Syzdykbayev et al., 2020a). Features of interest are defined by shape, size, or placement in the landscape that distinguishes them from other landscape features. One way of identifying a feature is by its height relative to the surrounding landscape. While conceptually straightforward, calculating feature height generally first requires identifying features. Here, we use a construction from TDA called *persistence* which simultaneously extracts topographic features and related information, from which we can calculate feature height, areal extent, and many other shape metrics.

To do this, we employ the main algorithm of the TDA package Ripser (Bauer, 2021; Tralie et al., 2018). Ripser computes persistent homology efficiently and is commonly used to analyze images, point clouds, and time series. Besides the ability to incorporate flexible underlying geometry, we have chosen to work with Ripser because it uses a fast agglomerative clustering algorithm in the 0th dimension and allows for our method to extend to data sets of different shapes and higher dimensions with little modification. In this study, we do not perform any preprocessing to remove slope or any other features. The only input to the algorithm is an elevation raster, treated as a 2-D array without geospatial reference.

When applied to an elevation array (example in Figure 2a), persistence consecutively thresholds the image at every data value (example thresholded images at the top of Figure 2c). From each binary thresholded image, an adjacency graph is constructed by placing a node in each colored pixel and connecting all adjacent nodes with edges (middle row of Figure 2c). At each threshold value, the set of connected components of the graph is identified; the components individually evolve in size and shape as the threshold changes, and the number of components grows and shrinks as the algorithm moves along the continuum of thresholds. This time-varying network of connected components is called a filtration or filtered simplicial complex. For details, see Text S1 in Supporting Information S1.

A feature is *born* at threshold t when a new isolated pixel group, corresponding to a new graph component, appears for the first time. When two graph components merge, the feature with a later birth threshold *dies* by convention, and the feature with an earlier birth threshold persists. The lifespan of a component or feature is visualized at the bottom of Figure 2c. Each horizontal bar spans from the birth threshold to the death threshold along which a feature is distinguishable from its surroundings in the binary map. The difference between the birth and death thresholds for a component is the apparent height of a feature relative to the surrounding area. For any vertical dashed line, all of the horizontal bars intersected represent components that appear in the above thresholded image and adjacency graph. As the threshold increases along the x -axis in Figure 2, features appear and merge until the whole image is a single feature. The full set of components that appear throughout this process are summarized in a persistence diagram (Figure 2b), which describes the elevation at which a feature first appears (its birth threshold) and its height (“persistence”). A feature is said to have infinite persistence if it persists through the full range of elevations present in the data. This does not imply that the feature exists at all possible threshold values but that the endpoint cannot be defined because they are outside the bounds of the image.

The persistence of features also indicates the sensitivity of results to a change in resolution. Low-persistence features may be sensitive to resolution changes, whereas high-persistence features are likely to be less sensitive to image resolution since they stand out more from their surroundings. Spatial resolution has been shown to affect the results of many spatial analyses (e.g., Irons et al., 1985; Ozonoff et al., 2007). Generally, reducing spatial resolution tends to smooth out differences in elevation since it results in a single value for a larger area. If features are substantially larger than the resolution, then this effect is minimal, but this effect can become important as the image resolution approaches the size of the feature. As long as there is still a marked difference in pixel values between the feature and the surroundings, though, it will be detected with persistence.

The persistence pipeline can be performed as either a *sub-level set filtration* where thresholding begins from the smallest value and increases or a *super-level set filtration*, which begins from the largest value and decreases. Figure 2 shows a sub-level set filtration. Like water slowly filling the landscape from the bottom up, the regions at lowest elevation are joined by points at increasing elevation until the entire landscape is below the threshold. This filtration is ideal for detecting features that are lower than their surroundings, such as stock ponds. In contrast, a super-level set filtration is ideal for detecting features that are higher than their surroundings, such as berms. All results in this study are found using a super-level set filtration.

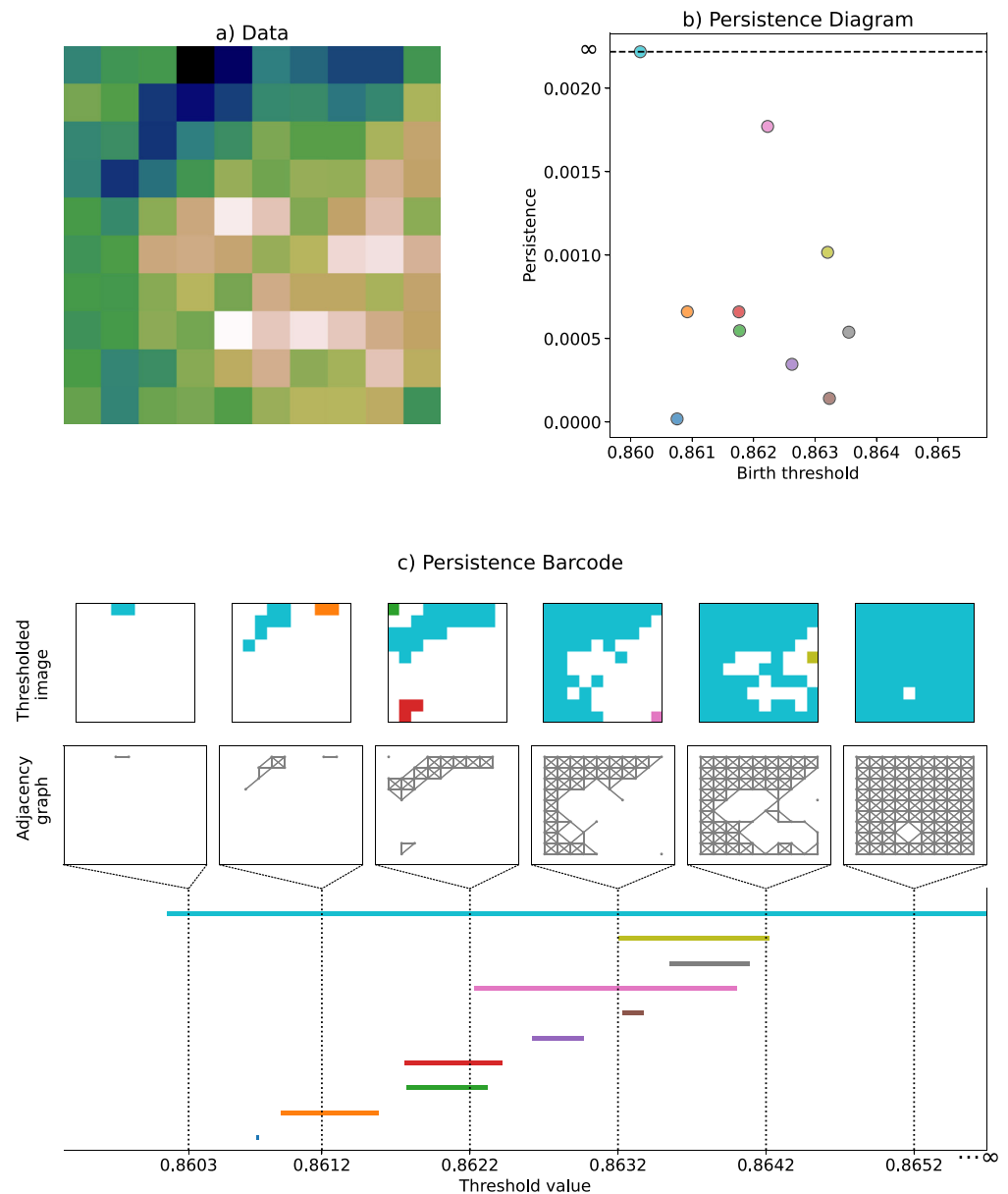


Figure 2. The persistent components of the sub-level set filtration of a randomly-generated example 10×10 digital terrain model, shown in (a). This figure demonstrates how persistence functions on an elevation array. The data is thresholded at all possible elevations, six example thresholded images shown at the top of (c). Each thresholded image is translated into an adjacency graph (middle row of panel c), with a node for each pixel and edges representing adjacency of pixels. The bars in the persistence barcode (bottom panel of c) record the interval of threshold values at which an isolated connected component exists in the thresholded image. The bars are represented in (b) by the left endpoint of the bar (“birth”) on the x -axis, and the length of the bar (“persistence”) on the y -axis. The components are color-coded across panels (c) and (b).

Figure 3 shows calculated persistence diagrams for four simple examples. Column (a) shows a smooth planar hillslope. With the super-level set filtration, as the binarization threshold is decreased from the highest value, a single feature grows continuously until it encompasses the whole image. The same happens with a sub-level set moving up from the bottom of the image. Thus, panels a2 and a3 both show only one feature, which is born at the starting threshold and persists infinitely. We added random noise to the slopes by using a pseudo-random number generator to add elevation to each point on the slope up to a maximum of 0.75 units. With random noise (b panels), the large main component similar to the a panels remains (b3-4, red point on dashed infinity line), but a lot of short-lived components appear and are absorbed into the large component quickly due to the noise. These

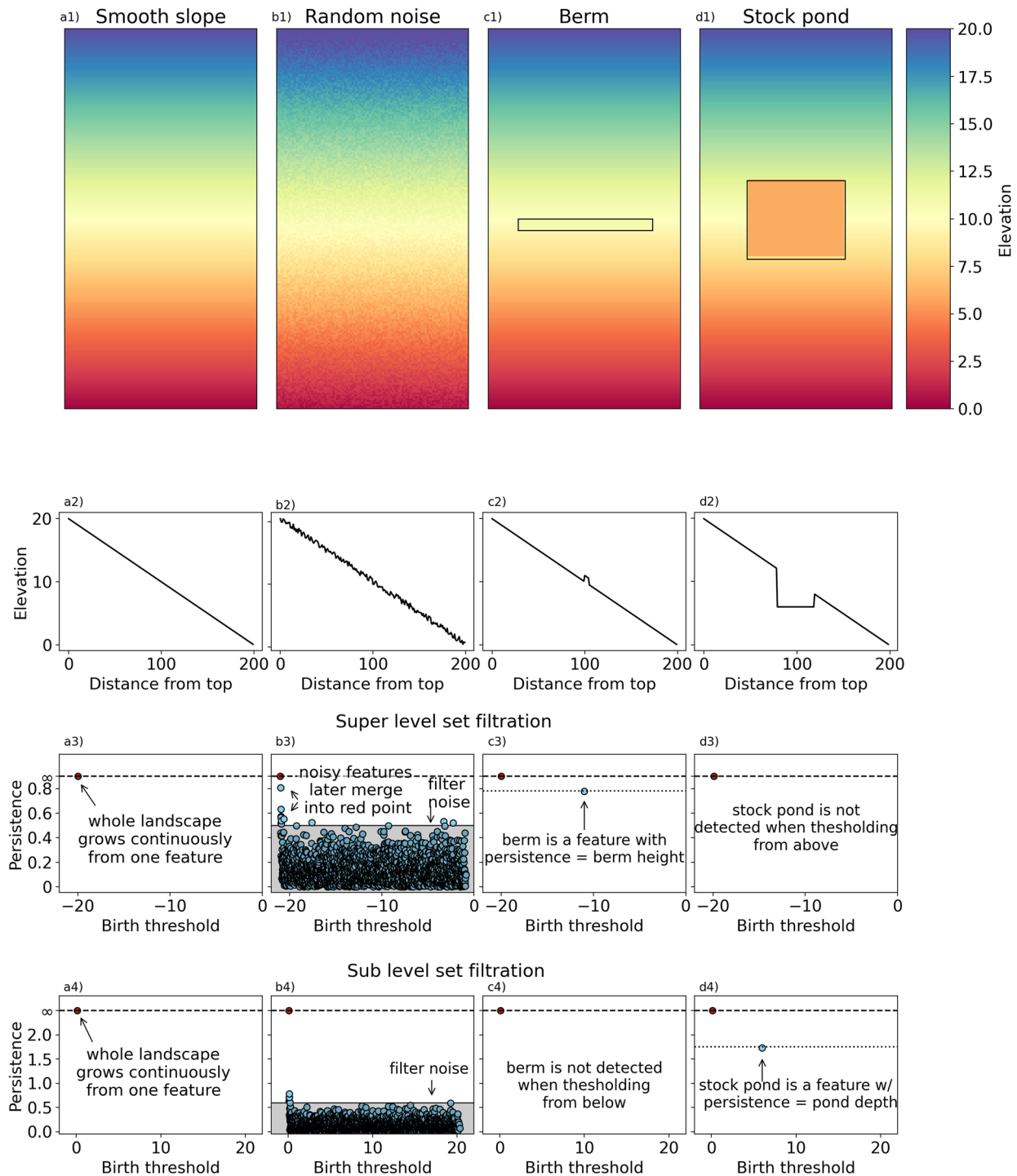


Figure 3. Synthetic example landscapes for (a) a smooth slope, (b) a slope with random noise, (c) a smooth slope with a berm, and (d) a smooth slope with a stock pond. The top row shows synthetic digital terrain models, the second row shows plan geometry, the third row shows persistent diagrams using a super level set filtration, and the bottom row shows persistent diagrams using a sub-level set filtration.

points generally fall below a noise threshold determined by the level of noise added to the slope (same threshold shown in Figures 3b3 and 3b4 as a shaded region). In general, noise can be filtered by removing components that have low persistence. Columns c and d show feature detection examples where c is a raised feature (berm), and d is a depressed feature (stock pond). To detect the berm in c, a super-level set filtration is needed (c3) so that as the filter threshold is decreased from above, the berm (blue dot) appears as a separate component from the main slope

(red dot). To understand why, imagine a horizontal bar dropping from the top of Figure 3c2, coloring the plan geometry as it moves down. When the bar first hits the berm, there is a discontinuity between the colored slope uphill of the berm and the colored high point on the berm. This indicates that the berm is identified as a separate feature. Now, imagine a horizontal bar rising from the bottom of the figure. When the bar contacts the berm, the colored line segment is connected from the berm down to the rest of the downslope landscape. This means that the berm is not identified as a separate feature. In contrast, a sub-level set filtration is needed to detect the stock pond (d4). This can be seen with a similar thought experiment. For more details on the persistence methodology, see Text S1 in Supporting Information S1.

Persistence is a specific technique; however, the same elevation-based spatial clustering of a digital elevation model can be achieved by *contour trees* and *surface networks*, constructions that are highly related to the zero-dimensional persistent homology (Rana, 2004). Contour trees offer a multi-level representation of terrain (Carr et al., 2003; Guilbert, 2013), from which specific topographical features can be identified. Compared to contour trees, which are specialized to surfaces, persistence can be adapted to maps of any shape, size, or dimension. Additionally, compared to vector-based contour tree methods, persistence computes hierarchy faster (Wu et al., 2019). The mathematical formulation used to calculate feature persistence also has several statistical advantages over simpler techniques. First, persistence guarantees stability under bounded perturbation of the data (Skraba & Turner, 2021). Functionally, this means that (a) an image noise threshold will match the threshold required to filter out noise from the persistence diagram and (b) that results are relatively insensitive to image resolution—persistence is invariant to upsampling (this corresponds to a simplicial *subdivision*, which is topologically invariant), and the difference caused by downsampling can be bounded by a constant (see Text S2 in Supporting Information S1). Second, topological persistence applies simultaneously across all scales with no required parameters. These benefits make persistence an ideal framework for application to feature detection.

Since we apply only 0th dimensional persistence in this work, our methods could be viewed simply as agglomerative clustering rather than invoking the larger theoretical structure of persistence. However, we choose to frame this work through the lens of persistence since it provides a more general framework that (a) may be useful for extensions of this work, (b) includes geometric results about the space of persistence diagrams, specifically confidence intervals, which may be relevant in larger-scale detection applications, and (c) we find persistence diagrams to be a useful way to visually present our results.

2.3. Persistence for Berm Detection

In the language of persistence, a berm is a persistent feature in a super-level set filtration where the height of the berm is given by the feature persistence. Inspection of the persistence diagram alone could reveal anomalous points, like the obvious points in Figures 3c2 and 3d3. However, if the size of features we are seeking to detect is known, then they can be identified using a threshold on persistence. For instance, if berms in a given region are approximately between 1 and 3 m high, features in a super level set filtration with a persistence from 1 to 3 m may be berms. We identified features by generating a binarized image where pixels are 1 if between the birth and death thresholds for a feature and otherwise 0. We performed a simple clustering algorithm on the binarized image and located the identified feature as the cluster overlapping the birth location of the feature as reported by Ripser.

However, Ripser does not compute birth locations for 0-dimensional persistence, which is what we used in this study. In the Ripser package, 0-dimensional persistence is implemented in a different computational engine than the higher-dimensional cohomology (see Text S1 for details in Supporting Information S1) and does not include birth location functionality. Thus, we extended the functionality of 0-dimensional cohomology to track the birth location of each feature. This update is available in the data supplement.

We performed two types of tests to assess feasibility of topological persistence for feature detection, one test to detect earthworks synthetically added to a DTM and one test using DTM clips containing real earthworks. All DTM tiles were created using Aerial LiDAR data (9–14 July 2016) sourced from Pima County Regional Flood Control district with 1 m spatial resolution and 10 cm vertical resolution. This resolution is adequate to resolve berms and stock ponds. Berms are generally 0.5–3 m high, 30–200 m long, and 2–4 m wide. For all examples, we identified berms as features of persistence between 0.4 and 3 m high to capture the range of real berm heights, which are typically 0.4–3 m high. However, there are many background features that fall in this range including channel banks, floodplain terraces, gully heads for incised channels, rocky hilltops, and anthropogenic features

Table 1
Summary of Constraints Used to Identify Features as Berms

Constraint	Min. value	Max. value	Description
Persistence	0.3 m	3 m	Ripser
Feature size	200 m ²	2,000 m ²	Number of pixels in feature
Feature length	40 m	250 m	Furthest distance between two points in feature
Feature width		15 m	Feature size/feature length
Feature height ratio	1	5	Average feature height/persistence
Feature length/width	6		
Distance to image boundary	7 m		Distance from birth location to nearest image boundary

like hay bales or piles of tires. To reduce noise, we introduced extra constraints for berm identification. We filtered by feature size to remove very small and very large features. Size was conservatively restricted between 200 and 2,000 m². The minimum boundary may exclude smaller berms, but these are of less interest for management applications since they would not have a large impact on hydrological processes. We also filtered by feature length, calculated as the maximum distance between points in a feature, which we restricted between 40 and 250 m. We further filtered by feature width, calculated as feature area/feature length, which we restricted to less than 15 m for berms, since berms tend to be 7–12 m wide. We also filtered by average feature height since berms have a shape that should make the average height about one third of the berm height. To do this we constrained the ratio between feature persistence and average feature height to between 1 and 5. Finally, we added a constraint on feature shape by ensuring that the feature is at least 6 times longer than it is wide, forcing features to be shaped like berms. We also neglected all features within 7 m of the edge of the DTM, since the image boundaries cause noise. A summary of the constraints is found in Table 1.

For all tests, we assess performance using precision (PC):

$$PC = \frac{TP}{TP + FP} \times 100 \quad (1)$$

where TP is the number of true positives (features detected that are actually berms) and FP is the number of false positives (features detected that are not berms) and detection rate (DT):

$$DT = \frac{N_D}{N_R} \times 100, \quad (2)$$

where N_D is the number of TP detected berms, and N_R is the number of reference objects identified manually.

2.3.1. Detection of Synthetic Berms

For initial proof-of-concept and to develop an understanding of how persistence may function on berms, we assessed the ability of persistence to identify berms by comparing the persistent diagrams for an unaltered DTM tile (location shown in Figure 1) and four separate versions of the DTM tile with synthetically added berms. These tests were done using unaltered landscapes located at numbers 1 and 2 in Figure 1a. For the first altered DTM (uniform height berms) Berms were added to the DTMs by adding 2–3 m to grid elevation values along lines that represent the berms. The locations and density of synthetic berms were designed to be similar to locations and density of real berms on the landscape. Berms are often placed along elevation contours, perpendicular to gullies to spread flow from gullies onto the downstream area. In many areas with berms, there are many berms built close to one another. By comparison with DTM tiles containing real berms and aerial imagery, we added an appropriate number of berms along contours at intervals along the existing gully network (8 for each site). The added berms had consistent size and uniform height, making them ideal targets for detection. The second example (tapered berms) again starts from the uniform height berm case but tapers the berm height down to ground level on the edges. For each berm, the middle third of the berm is constant height, and each end drops elevation in 0.25 m increments to ground level. The third example (breached berms) adds an eroded channel through each berm aligned with a drainage in the DTM. Breached berms are very common on the landscape and may be detected as multiple berms using persistence due to the channel dividing the berm. Berms also may not be detected if the

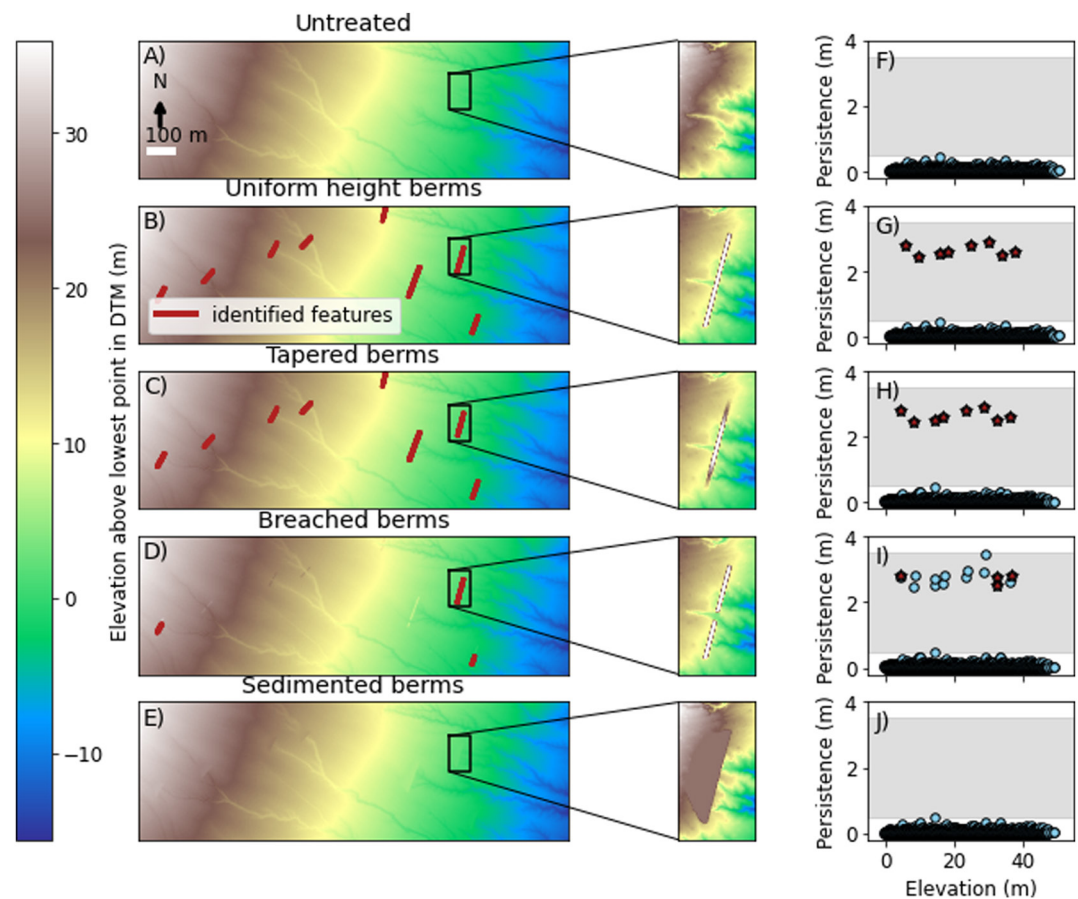


Figure 4. Digital terrain model (DTM) of area with no earthworks (a) located at number 1 in Figure 1a and the same area with synthetically added earthworks (b–e). Red lines in (b–e) mark locations of manually added berms identified with persistence. The enlarged berm shows a more detailed view of features identified with persistence in each case. Panels (f–j) are persistence diagrams for the original DTM (f) and altered DTMs (g–j). Features marked with red stars are detected as berms using the criteria in Table 1.

portions on either side of the breach are too small to meet the constraints outlined in Table 1. The height of the berm may also be detected differently due to its adjacency to the gully. The fourth example (sedimented berms) uses the same berm locations but with heights of 0.5 m. The upslope ground level is increased to form a terrace behind the berm, representing an end-of-life case for a berm that has backfilled with sediment. Because of the uphill aggradation of the landscape, we expected that these berms will not be detected as individual features using persistence. For a visual representation of each case, see the insets in Figures 4 and 5. In all synthetic examples, we had perfect knowledge of the locations, number of berms, and height of berms in the tile. Additionally, this method allowed for a direct comparison of the persistence diagram with and without berms for the same landscape, a comparison that is impossible with real DTM tiles which either have berms or do not have berms. The results of this analysis are valuable for understanding why persistence does or does not work on real berms.

2.3.2. Detection of Real Berms

For the second test, we compiled a set of DTM clips containing manually identified berms from locations A, B, and C in Figure 1a and the right box in the inset to Figure 1a (7.0 km², 11 berms). See Table 2 for site details. Berms were manually identified if they are at least 40 m long and 0.5 m high, to match the constraints on the algorithmic process. The minimum bound for persistence is slightly lower (0.3 m) to account for the fact that persistence may be less than berm height if there are irregularities in the land surrounding the berm. Since real berms are less uniform and less perfectly placed along contours than the synthetic berms, they are more difficult to detect. Many real berms also contain breaches and other erosion features that could impact the efficacy of the detection algorithm. Thus, it was necessary to apply persistence to DTMs containing real features to demonstrate its utility for feature detection.

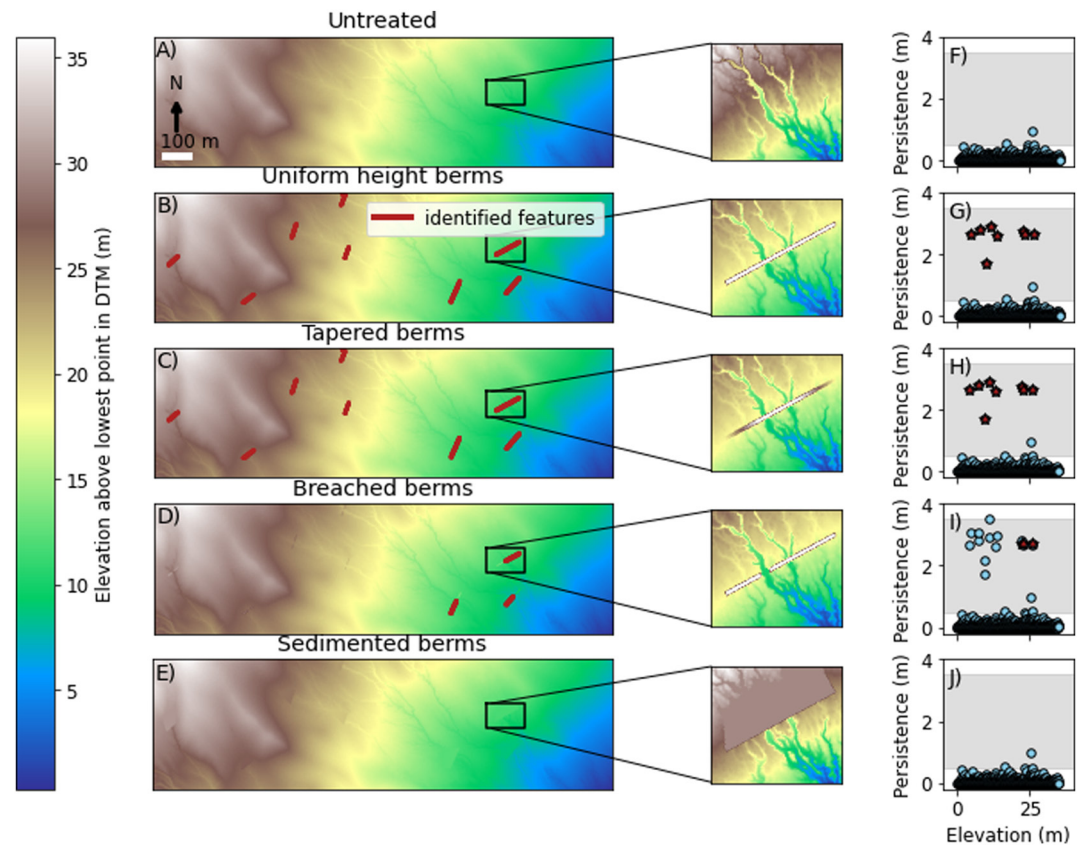


Figure 5. Digital terrain model (DTM) of area with no earthworks (a) located at number 2 in Figure 1a and the same area with synthetically added earthworks (b–e). Red lines in (b–e) mark locations of manually added berms identified with persistence. The enlarged berm shows a more detailed view of features identified with persistence in each case. Panels (f–j) are persistence diagrams for the original DTM (f) and altered DTMs (g–j). Features marked with red stars are detected as berms using the criteria in Table 1.

2.4. When Does Persistence Not Detect Berms?

To better understand why persistence detects some berms and not others, we manually collected data on all berms manually identified in the real berm detection examples including: berm length, berm width, berm shape, state of repair, maximum pixel value along the berm, maximum pixel value adjacent to the berm, and whether or not the berm was detected using persistence. All data were collected manually in QGIS so that the methods were identical for berms identified with persistence and not identified with persistence. Berm shape and state of repair were determined visually. Berm shape is a categorical variable with options: line, chevron, curved, pond, hooked, or t-shape. Most berms are linear. Chevron-shaped berms are pointed downstream in the middle. Curved berms arc to follow a contour. Pond berms are attached to stock ponds or form stock pond walls. Hooked berms are linear with a short extra linear feature attached to one end at an angle. T-shape berms have an extra extension perpendicular to the berm pointed upslope. State of repair is also categorical with the options: good, flank, or breach. Good berms show no significant visible erosion. Flanked berms have eroded gullies around one or both sides of the berm. Breached berms have an eroded path through the berm. We chose to collect maximum pixel value in berm and adjacent to berm rather than berm height because the difference between these values should be the berm height as detected using persistence. Berm shape, length, and state of repair can

Table 2
Detection Results for Each Region

Label in Figure 1a	Subplot in Figure 6	Area (km ²)	No. Berms	TP	FP	PC (%)	DT (%)
A	A	15.7	18	12	0	100	67
B	C	15.6	38	22	1	96	58
C	E	26.3	35	24	7	77	69
D ^a	G	7.0	12	8	6	57	67
Total		64.6	103	66	14	83	64

Note. TP is the number of berms detected as true positives using persistence along with the selection criteria in Table 1 FP is the number of features detected that are not berms. PC and DT are precision and detection rate as defined by Equations 1 and 2.

^aThis site is located with a blue box in the inset to Figure 1a.

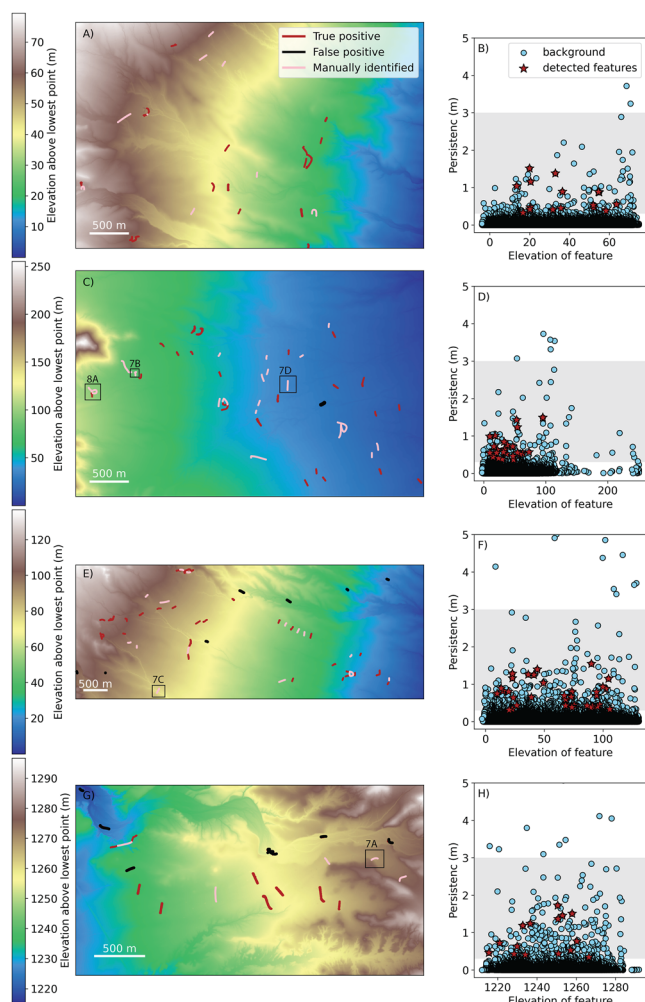


Figure 6. Results of feature detection on four real landscape tiles. See Table 2 for statistics and site details. Black boxes in subplots C, E, and G denote berms shown as examples in Figures 7 and 8. Each box is labeled with the Figure subplot where the example is shown. Gray shaded regions in subplots B, D, F, and H mark the persistence threshold used to identify berms. Red stars denote the features that meet all detection criteria in addition to the persistence criterion.

provide information about why a berm may not have passed the feature shape and size criteria used to reduce noise.

3. Results

3.1. Synthetic Berm Detection

Persistence is highly effective at identifying synthetically added berms on real landscapes (Figures 4 and 5). For the Uniform height and Tapered berm cases (second and third rows of Figures 4 and 5), persistence identifies 100% of the synthetic berms and fully outlines each berm correctly (see insets in panels b and c) with no false positives (PC = 100%, DT = 100%). As shown by the persistence diagrams (right column), the persistence of each feature detected as a berm (red stars) falls in the expected height range of about 2–3 m high. For the Breached berm case (fourth row in Figures 4 and 5), each berm shows up as two separate features (one for each side of the breach, see inset in panel d). The length and size of the identified features is reduced since each berm is identified as two features. In only three cases is either feature large enough to pass the berm size criteria in Table 1. This means that most breached berms in this example do not meet the berm size or length criteria, meaning that only three berms are detected (PC = 100%, DT = 38%). In the final row of each figure, no berms are detected. This suggests that berms at the end of their useful life will not be detected using persistence, whereas new berms and eroded berms may be detected, although breached berms may only be detected if the original berm is long or the breach is near the edge of the berm.

3.2. Detection of Real Berms

Persistence along with the feature selection criteria in Table 1 identified about two thirds of real berms across four sites (Figure 6 and Table 2; PC = 83%, DT = 64% across all sites). Persistence alone would not be adequate to identify berms since too many landscape features have persistence in the range used to detect berms (0.4–3 m), as shown by the blue dots in the gray regions in Figures 6b, 6d, 6f, and 6h. Nearly all of these can be filtered out using the selection criteria in Table 1 that ensure the feature is shaped like a berm. Only a few false positives remain when using the selection criteria: 1 in Figure 6c, 7 in Figure 6e, and 6 in Figure 6g. Nearly all of these features are channel banks in large streambeds, where berms are not built due to high risk of overflow. Masking out these large channel networks would reduce false positives to 1 in Figure 6c, 3 in Figure 6e, and 1 in Figure 6g and would improve overall PC from 83% to 93%.

3.3. Which Berm Characteristics Make Berms Hard to Detect With Persistence?

By collecting information about berms that were not detected, we identified four main cases in which persistence in combination with the selection criteria described in Table 1 is unable to detect berms. Examples of each of these four cases are shown in Figure 7. The first case (Figure 7a) is if a berm is directly adjacent to a higher-elevation feature. In this case, as the persistence method walks down from higher elevation thresholds, the berm never shows up as an individual feature but immediately connects to the higher-elevation feature next to it. This accounts for 6 of the 37 berms not detected. The second case is that the shape of a berm is unusual enough that it does not meet the selection criteria. This can happen if the berm is close to the length requirement of 40 m but not linear, as shown in Figure 7b or if a berm is actually a stock pond wall. This accounts for 4 of the 37 berms not detected. The third case is when a berm is breached so that no section of the berm is shaped properly to meet the selection criteria, usually because the sections are shorter than 40 m. This accounts for 3 of the 37 berms not detect. The fourth and most important case is when sedimentation upslope of the berm results

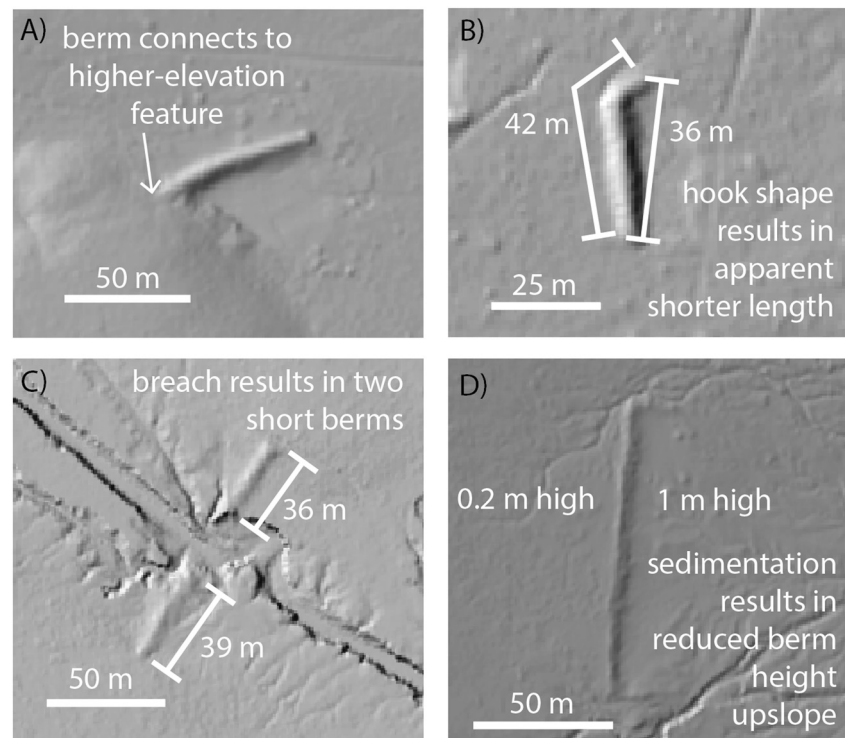


Figure 7. Examples showing the four main ways that persistence fails to detect berms. (a) The berm is connected to a higher-elevation feature. (b) Non-linear berm shape results in an apparent berm length that is shorter than the 40 m threshold used in this study. (c) A berm is breached, resulting in multiple berm pieces, none of which meets the minimum length threshold of 40 m. (d) Sedimentation upslope of the berm results in a significantly reduced berm height on the upslope side, reducing apparent berm height below the 0.4 m threshold used in this study. Locations of berms are shown in Figure 6 with black boxes and the corresponding panel label for this figure.

in reduced berm height upslope. In this case, the apparent berm height does not meet the persistence criteria, although the originally designed berm is much higher. This accounts for 21 of the 37 berms not detected. Given that this is the most prevalent case, it is unsurprising that the mean apparent height of detected berms is 0.7 m, while the mean apparent height of undetected berms is 0.2 m. The difference between the means is statistically significant ($p = 0.0002$). One of the remaining three undetected berms is significantly off-contour (not shown), which is harder to detect with persistence, since persistence functions by stepping through level sets or contours. The situations we identified account for 95% of berms that were not detected by persistence in this study. We

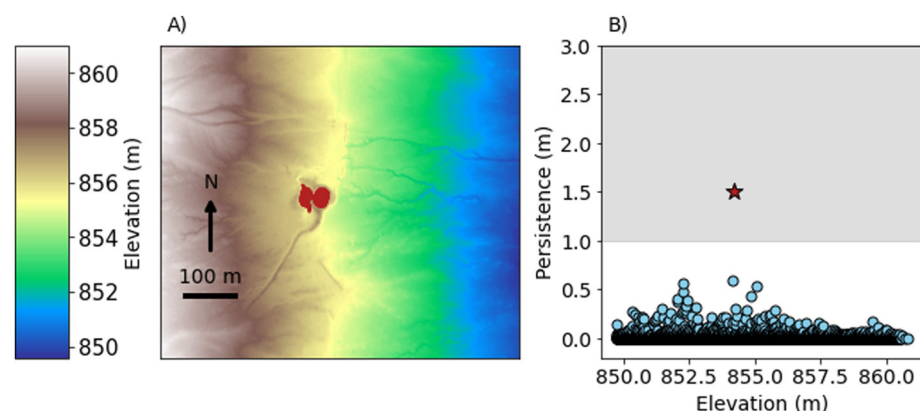


Figure 8. Demonstration that persistence can be used to detect stock ponds directly with a sub-level set filtration. The location of the stock pond shown in panel (a) is marked in Figure 6 with the label “8A.” The shaded gray region in (b) shows a higher threshold for feature detection than used for berms since stock ponds are generally deeper than berms are high.

could not determine why the last two berms were not detected, but these berms were located adjacent to one another in space, so the cause is likely the same for both berms and potentially site-specific.

4. Discussion

In this study, we applied persistence to identify earthworks in rangelands. On real landscapes, berms were identified from their surroundings using persistence (Figure 6) combined with feature shape criteria (Table 1) with an overall precision of $PC = 83\%$ and detection rate of $DT = 64\%$ across four sites containing a total of 103 berms. By masking out large stream channels, precision can be improved to 93%. Further improvements to precision could be made by incorporating other kinds of metrics such as a topographic position index (Wilson & Gallant, 2000). Synthetic berm detection tests as well as exploration of real berms not detected by persistence indicate that persistence is most effective at detecting berms in good repair or with flank erosion. Breached berms and sedimented berms may not be detected. This suggests that persistence is very effective for identifying well-maintained or new berms but is also effective enough on unmaintained berms to identify areas where earthworks are implemented. Earthworks tend to be constructed in spatially organized groups, so persistence could at least identify localized areas that would require additional manual or automated mapping to delineate earthworks not detected with persistence. These results are promising but do not represent a complete solution for automatic earthwork detection. Ongoing work is exploring the use of machine vision methods such as Geomorphon (Jasiewicz & Stepinski, 2013) for earthwork detection. A combination of detection methods with different strengths and weaknesses may be ideal for earthwork detection at large spatial scales.

The most similar feature detection tasks in the literature are focused on identifying levees, which are a similar shape to berms but located in a different orientation and position on the landscape. For levee detection, Steinfeld et al. (2013) found that PC for image segmentation, DEM analysis, and integrated analysis methods was about 30%, 95%, and 80%, and DT was about 45%, 65%, and 50%. Object-oriented and pixel-based classification methods applied by Csatáriné Szabó et al. (2020) provided overall accuracies of 75%–80%. The PC and DT found using persistence rank among the highest-performing of the semi-automated methods they tested for levees. Both of these studies note the difficulty of distinguishing levees from other natural features, but a detailed discussion of where the detection methods fail is not included in either study. Further exploration of the strengths and weaknesses of different approaches may reveal ways of distinguishing different subtypes of features, which may be better suited to identification with different types of methods.

Previous work has demonstrated that earthworks have different impacts on the landscape when in good versus poor conditions. In general, earthworks may be useful to restore degraded rangelands (Stavi et al., 2020), but earthworks in poor condition may have the opposite of the desired effect. For instance, good condition terraces tend to reduce hydrologic connectivity and downstream discharge, whereas collapsed terraces increase hydrologic connectivity and enhance concentrated flow pathways (Arnáez et al., 2015; Meerkerk et al., 2009). A similar effect has been observed with berms; across four sites in Arizona, degraded berms were associated with the development of concentrated flow pathways (Nichols et al., 2021). Previous work suggests that almost half of lateral channel berms may be breached (Nichols & Degginger, 2021), so an important part of mapping berm locations is noting their state of repair. The results of this study indicate that berms in poor repair may be detected differently by persistence from those in good repair. For instance, a berm with a breach through the middle is detected as two features (neither of which may be identified as a berm), and a berm with significant upslope sedimentation is not detected at all. While these observations limit the detection of berms in the context of the current study, they could be used to develop methods for categorizing berms in an automated way. In combination with other methods for earthwork identification, future work could focus on using strengths of different detection methods to distinguish between different types (contour berm vs. off-contour berm) and conditions (good condition vs. breached vs. sedimented). Such detailed information would be even more useful to land managers than location alone and could serve as a basis for large-scale studies on earthwork longevity and the differing impacts on landscapes of earthworks in good versus poor condition.

In this study, we focused on detection of berms; however, there are other prevalent earthworks on the landscape, including stock ponds. Stock pond dams and basin sidewalls may be detected as berms, but direct detection of stock ponds is also possible by using persistence with a sub-level set filtration (thresholds in algorithm step from lowest to highest rather than from highest to lowest). Figure 8a shows an example of a stock pond found in the study area (location marked with the symbol “8A” in Figure 6). The red area shows the depression identified as a stock pond using persistence. As shown by the persistence diagram in Figure 8b, stock ponds may be more straightforward to identify with persistence than berms given that they tend to be deeper than berms are high, so

there is unlikely to be many background features with similar persistence. Future work could explore the utility of persistence for identifying other earthworks such as stock ponds.

For this work, we used a relatively small fraction of the functionality of persistence and the Ripser package in particular. Persistence is typically used to describe features in higher dimensions. Thus, the tools used in this study are only a starting point for potential future applications of persistence in hydrology and open the door for potential analysis in higher dimensions, such as first homology of a super-level set filtration to detect raised pond boundaries, or second homology of a density filtration to detect underground features, as in Herring et al. (2019) and Moon et al. (2019). Further, the persistence framework can accommodate higher-dimensional data, so future work could incorporate multiple types of data to improve classification. Although we worked with persistent homology using the Ripser package, it may be desirable to use more sophisticated TDA packages in future applications: see Otter et al. (2017) for a partial comparison of available software. In particular, applications of multi-parameter persistence, such as the techniques used in Chung et al. (2022) and Vipond et al. (2021) for image data, could provide enough robustness to more accurately identify partially-degraded berms and stock ponds.

5. Conclusion

Earthworks are a control on landscape runoff processes both when operating as intended and when in degraded condition. Landscape managers, therefore, require detailed knowledge of the locations and condition of earthworks in order to make informed management decisions. Earthworks are readily visible in visual imagery as well as elevation maps of the landscape. However, given the large number of earthworks worldwide, reliable methods for automated earthwork detection are needed. In this study, we explored the use of persistence, a method from the mathematical field of topology, for automated earthwork detection. We found that persistence can be used to detect earthen berms 83% precision (can be improved to 93% by masking out large channels) and 64% accuracy. While promising, these results do not demonstrate a complete solution to the problem of automated earthwork detection. Persistence may be a useful tool in a larger workflow developed for more complete earthwork detection. Further, the way that the persistence method functions may prove useful in future applications that distinguish between earthworks in good and degraded condition.

Data Availability Statement

All data and code produced for this study are available at <https://zenodo.org/badge/latestdoi/263125392> (Lapides et al., 2022) except for the four large landscape DTMs. LiDAR data for these DTMs are available through the USGS 3D Elevation Program (<https://www.usgs.gov/3d-elevation-program>).

Acknowledgments

We would like to thank Paola Passalacqua for useful discussion, Michelle Cavanaugh for GIS assistance, Octavia Crompton for feedback on an early draft, and Laura Turnbull and anonymous reviewers for feedback that greatly improved the manuscript. We thank the Pima County Regional Flood Control District for access to lidar data. This research is based upon work supported by the U.S. Department of Agriculture, Natural Resources Conservation Service, Conservation Effects Assessment Project-Grazing Lands component, under agreement number NR213A750023C013. Funding for DAL was provided by the USDA Forest Service Pacific Southwest Research Station with funds administered by Oak Ridge Institute for Science and Education (ORISE). GG gratefully acknowledges funding from the Centre for Topological Data Analysis, funded by the EPSRC Grant (EP/R018472/1), as well as NSF MSPRF 2202895.

References

- Adams, D. K., & Comrie, A. C. (1997). The North American monsoon. *Bulletin of the American Meteorological Society*, 78(10), 2197–2214. [https://doi.org/10.1175/1520-0477\(1997\)078<2197:tnam>2.0.co;2](https://doi.org/10.1175/1520-0477(1997)078<2197:tnam>2.0.co;2)
- Armáez, J., Lana-Renault, N., Lasanta, T., Ruiz-Flaño, P., & Castroviejo, J. (2015). Effects of farming terraces on hydrological and geomorphological processes. A review. *Catena*, 128, 122–134. <https://doi.org/10.1016/j.catena.2015.01.021>
- Arundel, S. (2016). Pairing semantics and object-based image analysis for national terrain mapping: A first-case scenario of cirques. In *6th international conference on geographic object-based image analysis, Geobia 2016: Solutions & synergies*.
- Atkinson, J., de Clercq, W., & Rozanov, A. (2020). Multi-resolution soil-landscape characterisation in kwazulu natal: Using geomorphons to classify local soilscapes for improved digital geomorphological modelling. *Geoderma Regional*, 22, e00291. <https://doi.org/10.1016/j.geodrs.2020.e00291>
- Bauer, U. (2021). Ripser: Efficient computation of vietoris-rips persistence barcodes. *Journal of Applied and Computational Topology*, 5(3), 391–423. <https://doi.org/10.1007/s41468-021-00071-5>
- Boers, T. M., & Ben-Asher, J. (1982). A review of rainwater harvesting. *Agricultural Water Management*, 5(2), 145–158. [https://doi.org/10.1016/0378-3774\(82\)90003-8](https://doi.org/10.1016/0378-3774(82)90003-8)
- Bonetto, S., Facello, A., Ferrero, A. M., & Umili, G. (2015). A tool for semi-automatic linear feature detection based on DTM. *Computers & Geosciences*, 75, 1–12. <https://doi.org/10.1016/j.cageo.2014.10.005>
- Bryan, K. (1929). Flood-water farming. *Geographical Review*, 19(3), 444–456. <https://doi.org/10.2307/209150>
- Campisano, A., Butler, D., Ward, S., Burns, M. J., Friedler, E., DeBusk, K., et al. (2017). Urban rainwater harvesting systems: Research, implementation and future perspectives. *Water Research*, 115, 195–209. <https://doi.org/10.1016/j.watres.2017.02.056>
- Carr, H., Snoeyink, J., & Axen, U. (2003). Computing contour trees in all dimensions. *Computational Geometry*, 24(2), 75–94. [https://doi.org/10.1016/S0925-7721\(02\)00093-7](https://doi.org/10.1016/S0925-7721(02)00093-7)
- Cheng, C.-T., & Chau, K.-W. (2004). Flood control management system for reservoirs. *Environmental Modelling & Software*, 19(12), 1141–1150. <https://doi.org/10.1016/j.envsoft.2003.12.004>
- Chung, Y.-M., Day, S., & Hu, C.-S. (2022). A multi-parameter persistence framework for mathematical morphology. *Scientific Reports*, 12(1), 6427. <https://doi.org/10.1038/s41598-022-09464-7>

- Corcoran, P. (2019a). Topological generalization of continuous valued raster data. In *Proceedings of the 27th ACM SIGSPATIAL international conference on advances in geographic information systems* (pp. 428–431). Association for Computing Machinery. <https://doi.org/10.1145/3347146.3359071>
- Corcoran, P. (2019b). Topology based object tracking. *Mathematical and Computational Applications*, 24(3), 84. <https://doi.org/10.3390/mca24030084>
- Corcoran, P., & Jones, C. B. (2018). Robust tracking of objects with dynamic topology. In *Proceedings of the 26th ACM sigspatial international conference on advances in geographic information systems* (pp. 428–431).
- Corcoran, P., & Jones, C. B. (2023). Topological data analysis for geographical information science using persistent homology. *International Journal of Geographical Information Science*, 37(3), 712–745. <https://doi.org/10.1080/13658816.2022.2155654>
- Csatáriné Szabó, Z., Mikita, T., Négyesi, G., Varga, O. G., Burai, P., Takács-Szilágyi, L., & Szabó, S. (2020). Uncertainty and overfitting in fluvial landform classification using laser scanned data and machine learning: A comparison of pixel and object-based approaches. *Remote Sensing*, 12(21), 3652. <https://doi.org/10.3390/rs12213652>
- Drăguț, L., & Eisank, C. (2012). Automated object-based classification of topography from SRTM data. *Geomorphology*, 141, 21–33. <https://doi.org/10.1016/j.geomorph.2011.12.001>
- Goldgof, D. B., Huang, T. S., & Lee, H. (1989). A curvature-based approach to terrain recognition. *IEEE Transactions on Pattern Analysis and Machine Intelligence*, 11(11), 1213–1217. <https://doi.org/10.1109/34.42859>
- Goldgof, D. B., Huang, T. S., & Lee, H. (1990). Terrain analysis from curvature profiles. *International Journal of Imaging Systems and Technology*, 2(3), 169–182. <https://doi.org/10.1002/ima.1850020303>
- Guilbert, E. (2013). Multi-level representation of terrain features on a contour map. *Geoinformatica*, 17(2), 301–324. <https://doi.org/10.1007/s10707-012-0153-z>
- Herring, A. L., Robins, V., & Sheppard, A. P. (2019). Topological persistence for relating microstructure and capillary fluid trapping in sandstones. *Water Resources Research*, 55(1), 555–573. <https://doi.org/10.1029/2018WR022780>
- Höfle, B., Griesbaum, L., & Forbriger, M. (2013). GIS-based detection of gullies in terrestrial LiDAR data of the Cerro Llamoca Peatland (Peru). *Remote Sensing*, 5(11), 5851–5870. <https://doi.org/10.3390/rs5115851>
- Hsu, C.-Y., Li, W., & Wang, S. (2021). Knowledge-driven GeoAI: Integrating spatial knowledge into multi-scale deep learning for mars crater detection. *Remote Sensing*, 13(11), 2116. <https://doi.org/10.3390/rs13112116>
- Irons, J. R., Markham, B. L., Nelson, R. F., Toll, D. L., Williams, D. L., Latty, R. S., & Stauffer, M. L. (1985). The effects of spatial resolution on the classification of thematic mapper data. *International Journal of Remote Sensing*, 6(8), 1385–1403. <https://doi.org/10.1080/01431168508948285>
- Jasiewicz, J., & Stepinski, T. F. (2013). Geomorphons—A pattern recognition approach to classification and mapping of landforms. *Geomorphology*, 182, 147–156. <https://doi.org/10.1016/j.geomorph.2012.11.005>
- Khan, S., & Shah, M. (2001). Object based segmentation of video using color, motion and spatial information. In *Proceedings of the 2001 IEEE computer society conference on computer vision and pattern recognition. CVPR 2001* (Vol. 2, p. II-II).
- Kramar, M., Levanger, R., Tithof, J., Suri, B., Xu, M., Paul, M., et al. (2016). Analysis of Kolmogorov flow and Rayleigh–Bénard convection using persistent homology. *Physica D: Nonlinear Phenomena*, 334, 82–98. <https://doi.org/10.1016/j.physd.2016.02.003>
- Lapides, D., Grindstaff, G., & Nichols, M. (2022). Supporting code and data for: Automated earthwork detection using topological persistence. *Zenodo*. Retrieved from <https://zenodo.org/badge/latestdoi/263125392>
- Li, M., An, H., Angelovici, R., Bagaza, C., Batushansky, A., Clark, L., et al. (2018). Topological data analysis as a morphometric method: Using persistent homology to demarcate a leaf morphospace. *Frontiers in Plant Science*, 9, 553. <https://doi.org/10.3389/fpls.2018.00553>
- Lindsay, J. B., & Dhun, K. (2015). Modelling surface drainage patterns in altered landscapes using lidar. *International Journal of Geographical Information Science*, 29(3), 397–411. <https://doi.org/10.1080/13658816.2014.975715>
- Liu, X., & Zhang, Z. (2011). Drainage network extraction using LiDAR-derived DEM in volcanic plains. *Area*, 43(1), 42–52. <https://doi.org/10.1111/j.1475-4762.2010.00955.x>
- Meerkerk, A., van Wesemael, B., & Bellin, N. (2009). Application of connectivity theory to model the impact of terrace failure on runoff in semi-arid catchments. *Hydrological Processes: International Journal*, 23(19), 2792–2803. <https://doi.org/10.1002/hyp.7376>
- Molloy, I., & Stepinski, T. F. (2007). Automatic mapping of valley networks on mars. *Computers & Geosciences*, 33(6), 728–738. <https://doi.org/10.1016/j.cageo.2006.09.009>
- Moon, C., Mitchell, S. A., Heath, J. E., & Andrew, M. (2019). Statistical inference over persistent homology predicts fluid flow in porous media. *Water Resources Research*, 55(11), 9592–9603. <https://doi.org/10.1029/2019WR025171>
- Myers, L. E. (1975). *Water harvesting—2000 BC to 1974 AD*. ARS W Agricultural Research Service US Department of Agricultural.
- Naik, S. K., & Murthy, C. (2006). Standardization of edge magnitude in color images. *IEEE Transactions on Image Processing*, 15(9), 2588–2595. <https://doi.org/10.1109/tip.2006.877408>
- Nichols, M. H., & Degginger, T. (2021). The landscape impact of unmaintained rangeland water control structures in southern Arizona, USA. *Catena*, 201, 105201. <https://doi.org/10.1016/j.catena.2021.105201>
- Nichols, M. H., Magirl, C., Sayre, N. F., & Shaw, J. R. (2018). The geomorphic legacy of water and erosion control structures in a semiarid rangeland watershed. *Earth Surface Processes and Landforms*, 43(4), 909–918. <https://doi.org/10.1002/esp.4287>
- Nichols, M. H., Shaw, J. R., & Brandau, W. K. (2021). Unintended consequences of rangeland conservation structures. *International Soil and Water Conservation Research*, 9(1), 158–165. <https://doi.org/10.1016/j.iswcr.2020.11.006>
- Otter, N., Porter, M. A., Tillmann, U., Grindrod, P., & Harrington, H. A. (2017). A roadmap for the computation of persistent homology. *EPJ Data Science*, 6, 1–38. <https://doi.org/10.1140/epjds/s13688-017-0109-5>
- Ozonoff, A., Jeffery, C., Manjournides, J., White, L. F., & Pagano, M. (2007). Effect of spatial resolution on cluster detection: A simulation study. *International Journal of Health Geographics*, 6, 1–7. <https://doi.org/10.1186/1476-072x-6-52>
- Pandey, D. N., Gupta, A. K., & Anderson, D. M. (2003). Rainwater harvesting as an adaptation to climate change. *Current Science*, 85, 46–59.
- Passalacqua, P., Tarolli, P., & Foufoula-Georgiou, E. (2010). Testing space-scale methodologies for automatic geomorphic feature extraction from lidar in a complex mountainous landscape. *Water Resources Research*, 46(11), W11535. <https://doi.org/10.1029/2009wr008812>
- Rana, S. (2004). *Topological data structures for surfaces*. Wiley Online Library.
- Saraf, A. K., Choudhury, P., Roy, B., Sarma, B., Vijay, S., & Choudhury, S. (2004). GIS based surface hydrological modelling in identification of groundwater recharge zones. *International Journal of Remote Sensing*, 25(24), 5759–5770. <https://doi.org/10.1080/0143116042000274096>
- Sills, G., Vroman, N., Wahl, R., & Schwanz, N. (2008). Overview of New Orleans levee failures: Lessons learned and their impact on national levee design and assessment. *Journal of Geotechnical and Geoenvironmental Engineering*, 134(5), 556–565. [https://doi.org/10.1061/\(asce\)1090-0241\(2008\)134:5\(556\)](https://doi.org/10.1061/(asce)1090-0241(2008)134:5(556))
- Skraba, P., & Turner, K. (2021). Wasserstein stability for persistence diagrams.

- Soille, P., & Pesaresi, M. (2002). Advances in mathematical morphology applied to geoscience and remote sensing. *IEEE Transactions on Geoscience and Remote Sensing*, 40(9), 2042–2055. <https://doi.org/10.1109/tgrs.2002.804618>
- Stavi, I., Siad, S., Kyriazopoulos, A., & Halbac-Cotoara-Zamfir, R. (2020). Water runoff harvesting systems for restoration of degraded rangelands: A review of challenges and opportunities. *Journal of Environmental Management*, 255, 109823. <https://doi.org/10.1016/j.jenvman.2019.109823>
- Steinfeld, C. M., & Kingsford, R. T. (2013). Disconnecting the floodplain: Earthworks and their ecological effect on a dryland floodplain in the Murray–Darling Basin, Australia. *River Research and Applications*, 29(2), 206–218. <https://doi.org/10.1002/rra.1583>
- Steinfeld, C. M., Kingsford, R. T., & Laffan, S. W. (2013). Semi-automated GIS techniques for detecting floodplain earthworks. *Hydrological Processes*, 27(4), 579–591. <https://doi.org/10.1002/hyp.9244>
- Suzuki, A., Miyazawa, M., Minto, J. M., Tsuji, T., Obayashi, I., Hiraoka, Y., & Ito, T. (2021). Flow estimation solely from image data through persistent homology analysis. *Scientific Reports*, 11(1), 17948. <https://doi.org/10.1038/s41598-021-97222-6>
- Syed Musa, S. M. S., Md Noorani, M. S., Abdul Razak, F., Ismail, M., Alias, M. A., & Hussain, S. I. (2021). Using persistent homology as preprocessing of early warning signals for critical transition in flood. *Scientific Reports*, 11(1), 7234. <https://doi.org/10.1038/s41598-021-86739-5>
- Szydkbayev, M., Karimi, B., & Karimi, H. A. (2020a). A method for extracting some key terrain features from shaded relief of digital terrain models. *Remote Sensing*, 12(17), 2809. <https://doi.org/10.3390/rs12172809>
- Szydkbayev, M., Karimi, B., & Karimi, H. A. (2020b). Persistent homology on LiDAR data to detect landslides. *Remote Sensing of Environment*, 246, 111816. <https://doi.org/10.1016/j.rse.2020.111816>
- Tadmor, N., Shanan, L., & Evenari, M. (1971). “runoff farming” in the desert. V. persistence and yields of annual range species 1. *Agronomy Journal*, 63(1), 91–95. <https://doi.org/10.2134/agronj1971.00021962006300010028x>
- Tarolli, P. (2014). High-resolution topography for understanding earth surface processes: Opportunities and challenges. *Geomorphology*, 216, 295–312. <https://doi.org/10.1016/j.geomorph.2014.03.008>
- Tarolli, P., Sofia, G., Calligaro, S., Prosdoci, M., Preti, F., & Dalla Fontana, G. (2015). Vineyards in terraced landscapes: New opportunities from lidar data. *Land Degradation & Development*, 26(1), 92–102. <https://doi.org/10.1002/ldr.2311>
- Tarolli, P., Sofia, G., & Dalla Fontana, G. (2012). Geomorphic features extraction from high-resolution topography: Landslide crowns and bank erosion. *Natural Hazards*, 61(1), 65–83. <https://doi.org/10.1007/s11069-010-9695-2>
- Torres, R. N., Fraternali, P., Milani, F., & Frajberg, D. (2020). Mountain summit detection with deep learning: Evaluation and comparison with heuristic methods. *Applied Geomatics*, 12(2), 225–246. <https://doi.org/10.1007/s12518-019-00295-2>
- Tralie, C., Saul, N., & Bar-On, R. (2018). Ripser. Py: A lean persistent homology library for python. *Journal of Open Source Software*, 3(29), 295. <https://doi.org/10.21105/joss.00925>
- Tymochko, S., Munch, E., Dunion, J., Corbosiero, K., & Torn, R. (2020). Using persistent homology to quantify a diurnal cycle in hurricanes. *Pattern Recognition Letters*, 133, 137–143. <https://doi.org/10.1016/j.patrec.2020.02.022>
- Vipond, O., Bull, J. A., Macklin, P. S., Tillmann, U., Pugh, C. W., Byrne, H. M., & Harrington, H. A. (2021). Multiparameter persistent homology landscapes identify immune cell spatial patterns in tumors. *Proceedings of the National Academy of Sciences*, 118(41), e2102166118. <https://doi.org/10.1073/pnas.2102166118>
- Wang, S., & Li, W. (2021). GeoAI in terrain analysis: Enabling multi-source deep learning and data fusion for natural feature detection. *Computers, Environment and Urban Systems*, 90, 101715. <https://doi.org/10.1016/j.compenvurbsys.2021.101715>
- Wilson, J. P., & Gallant, J. C. (2000). Secondary topographic attributes. In *Terrain analysis: Principles and applications* (pp. 87–131).
- Wilson, J. P., Gallant, J. C., & Hutchinson, M. F. (2000). Digital terrain analysis. In *Terrain analysis: Principles and applications no. 12* (Vol. 6, pp. 1–27).
- Wu, Q., Lane, C. R., Wang, L., Vanderhoof, M. K., Christensen, J. R., & Liu, H. (2019). Efficient delineation of nested depression hierarchy in digital elevation models for hydrological analysis using level-set method. *JAWRA Journal of the American Water Resources Association*, 55(2), 354–368. <https://doi.org/10.1111/1752-1688.12689>
- Xiong, L., Tang, G., Yang, X., & Li, F. (2021). Geomorphology-oriented digital terrain analysis: Progress and perspectives. *Journal of Geographical Sciences*, 31(3), 456–476. <https://doi.org/10.1007/s11442-021-1853-9>
- Zhang, S., You, S., Chen, L., & Liu, X. (2020). Analysis of tunnel failure characteristics under multiple explosion loads based on persistent homology-based machine learning. *arXiv*. <https://doi.org/10.48550/ARXIV.2009.10069>
- Zhang, S., Zhao, B., & Erdun, E. (2014). Watershed characteristics extraction and subsequent terrain analysis based on digital elevation model in flat region. *Journal of Hydrologic Engineering*, 19(11), 04014023. [https://doi.org/10.1061/\(asce\)he.1943-5584.0000961](https://doi.org/10.1061/(asce)he.1943-5584.0000961)
- Zhou, X., Li, W., & Arundel, S. T. (2019). A spatio-contextual probabilistic model for extracting linear features in hilly terrains from high-resolution DEM data. *International Journal of Geographical Information Science*, 33(4), 666–686. <https://doi.org/10.1080/13658816.2018.1554814>

References From the Supporting Information

- Cohen-Steiner, D., Edelsbrunner, H., & Harer, J. (2007). Stability of persistence diagrams. *Discrete & Computational Geometry*, 37(1), 103–120. <https://doi.org/10.1007/s00454-006-1276-5>
- de Silva, V., Morozov, D., & Vejdemo-Johansson, M. (2011). Dualities in persistent (co)homology. *Inverse Problems*, 27(12), 124003. <https://doi.org/10.1088/0266-5611/27/12/124003>
- Hatcher, A. (2002). *Algebraic topology*. Cambridge University Press. Retrieved from <https://books.google.co.uk/books?id=BjKs86kosqgC>
- Zomorodian, A., & Carlsson, G. (2005). Computing persistent homology. *Discrete & Computational Geometry*, 33(2), 249–274. <https://doi.org/10.1007/s00454-004-1146-y>